Geophysical Research Letters

RESEARCH LETTER
10.1029/2020GL088886

Can the Madden-Julian Oscillation Affect the Antarctic Total Column Ozone?

Chengyun Yang[1,2,3], Anne K. Smith[4], Tao Li[1,2,3], Douglas E. Kinnison[4], Jianghanyang Li[5], and Xiankang Dou[1,2,3,6]

[1]CAS Key Laboratory of Geospace Environment, School of Earth and Space Sciences, University of Science and Technology of China, Hefei, Anhui, China, [2]Mengcheng National Geophysical Observatory, School of Earth and Space Sciences, University of Science and Technology of China, Hefei, Anhui, China, [3]CAS Center for Excellence in Comparative Planetology, University of Science and Technology of China, Hefei, Anhui, China, [4]Atmospheric Chemistry Observation and Modeling, National Center for Atmospheric Research, Boulder, CO, USA, [5]Department of Earth, Atmospheric, and Planetary Sciences, Purdue University, West Lafayette, IN, USA, [6]School of Electronic Information, Wuhan University, Wuhan, Hubei, China

Key Points:
- Antarctic total column ozone significantly decreases at lags of 20–30 days after MJO Phase 8
- The MJO-related anomalous PWs propagate from the SH subtropics to the high latitudes and extend into the lower stratosphere
- The MJO P8 leads to a decrease in the poleward transport of ozone in the lower SH stratosphere

Supporting Information:
- Supporting Information S1

Correspondence to:
T. Li,
litao@ustc.edu.cn

Citation:
Yang, C., Smith, A. K., Li, T., Kinnison, D. E., Li, J., & Dou, X. (2020). Can the Madden-Julian Oscillation affect the Antarctic total column ozone? *Geophysical Research Letters*, *47*, e2020GL088886. https://doi.org/10.1029/2020GL088886

Received 20 MAY 2020
Accepted 15 JUL 2020
Accepted article online 29 JUL 2020

Abstract The effect of the Madden-Julian Oscillation (MJO) on springtime Antarctic ozone variations is revealed for the first time from multi-satellite reanalysis and model simulations. Twenty to 30 days after MJO Phase 8 (P8), Antarctic total column ozone (TCO) anomalies significantly decrease by up to −15 DU, associated with a wave-1 response at around 60°S. After MJO P8, MJO-related geopotential height anomalies in the southern hemispheric (SH) Indian Ocean emanate from subtropics to polar regions, leading to suppressed upward and poleward propagation of planetary waves (PWs) and weakened Brewer-Dobson circulation in the SH stratosphere. This in turn results in less ozone transport from midlatitudes into the polar region and thus a negative polar TCO response. Dynamical transport plays a dominant role in modulating the Antarctic TCO after MJO P8. The magnitude of transient changes due to chemical processes is relatively weak than that caused by dynamical transport.

Plain Language Summary This investigation explores how the southern hemispheric circulation and Antarctic ozone vary in response to a dominant tropospheric intraseasonal phenomenon known as the Madden-Julian Oscillation (MJO), which is characterized by globally coherent variations in tropical convective activity with a time scale ranging from 30 to 80 days. The MJO-related perturbations can modulate the atmospheric circulation in the southern hemispheric stratosphere. The deceleration of the atmospheric circulation in the lower stratosphere decreases the transport of ozone-rich air from lower latitudes to the polar region, which then leads to significant ozone perturbation over Antarctica after certain phases of the MJO.

1. Introduction

Stratospheric ozone protects life on Earth by strongly absorbing harmful solar ultraviolet radiation (Longstreth et al., 1995; Slaper et al., 1996; Van der Leun et al., 1995). It also plays an important role in modulating the global climate system by partly controlling the large-scale atmospheric circulation via its radiative impact and radiative-chemical-dynamical feedbacks (e.g., Calvo et al., 2015; Feldstein, 2011; Gillett et al., 2019; Kang et al., 2011; Smith et al., 2010; Son et al., 2008; Thompson et al., 2011; Xie et al., 2016). It has been well established that planetary waves (PWs) propagating into the stratosphere have considerable impact on the ozone hole through both dynamical and chemical processes (e.g., Fusco & Salby, 1999; Randel et al., 2002; Solomon, 1999) by modulating the residual circulation and the polar vortex. The sea surface temperature and convective activity variations in the tropics have been shown to modulate the lower-stratospheric ozone at southern high latitudes during the austral spring (e.g., Hurwitz et al., 2011, 2013; Lin et al., 2012; Tian et al., 2017).

The Madden-Julian Oscillation (MJO), which is the dominant mode of tropospheric intraseasonal oscillation, is characterized by a repeated eastward-propagating perturbation in deep convection and a coupled circulation (Madden & Julian, 1971, 1972) having a period of ~30–80 days (e.g., Zhang, 2005). Recent studies suggested that MJO-induced diabatic heating excites PWs at middle and high latitudes (Ferranti et al., 1990; Seo & Son, 2012) and, in turn, influences the stratosphere by modulating eddy momentum/heat transport

(Garfinkel et al., 2014; Kang & Tziperman, 2017, 2018). Observations (e.g., Wang et al., 2018; Yang et al., 2017) show variations in the circulation and temperature in the polar stratosphere of the Southern Hemisphere (SH) and Northern Hemisphere associated with several phases of the MJO.

Many studies have shown that enhanced upward PWs propagation into the Antarctic stratosphere leads to significant increases in total column ozone (TCO) and polar temperature in winter and subsequently less springtime ozone destruction in the stratosphere (e.g., Lin & Qian, 2019; Randel, 1993; Rose & Brasseur, 1985; Salby et al., 2011; Weber et al., 2011; Wirth, 1993). The cited studies focus on the long-term and interannual variability of stratospheric polar ozone, but we find that the Antarctic ozone averaged from 70°S to the pole also shows a significant variation on intraseasonal time scales (see Figure S1 in supporting information). The timing of the intraseasonal variability of Antarctic ozone and its possible coupling with the tropospheric intraseasonal MJO activities have not yet been well established. In this study, we explore the possible impacts of the MJO on the SH stratosphere residual circulation, Antarctic temperature, and ozone variation during the austral spring season (September–October–November, SON hereafter). A description of these linked perturbations will help us characterize the dynamical and chemical coupling mechanisms between the troposphere and stratosphere.

2. Data and Methods

The daily TCO data from the Ozone Multi-Sensor reanalysis version 2 (MSR-2) data set (van der A et al., 2010, 2015) from 1979 to 2014 are used in this paper. This detailed data set is produced by assimilating all independent satellite column observations publicly available (15 data sets in total: BUV-Nimbus4, TOMS-Nimbus7, TOMS-EP, SBUV-7, -9, -11, -14, -16, -17, -18, -19, GOME, SCIAMACHY, OMI, and GOME-2), with a horizontal resolution of 0.5° × 0.5° (latitude × longitude).

WACCM is a coupled chemistry-climate model (Garcia et al., 2007, 2017; Hurrell et al., 2013; Marsh et al., 2013), which is the high-top atmosphere component of the Community Earth System Model. In this study, we used data from a 36-year (1979–2014) simulation of the "Specific Dynamics" (SD) version of WACCM (SD-WACCM), version 4, to investigate the response of Antarctic ozone and related atmospheric variables to the MJO. SD-WACCM is nudged to meteorological fields from Modern-Era Retrospective Analysis for Research and Applications reanalysis data in the troposphere and stratosphere (from the surface to 1 hPa) (Kunz et al., 2011). With the relaxation, the MJO characteristics and the responses to it in the troposphere and stratosphere in SD-WACCM follow those in the reanalysis meteorological fields. This setup allows us to investigate both the physical and chemical processes involved in the response of the Antarctic ozone to observed MJO events.

The MJO phases are identified with the real-time multivariate MJO (RMM) index (available at http://www.bom.gov.au/climate/mjo/graphics/rmm.74toRealtime.txt) following the methods of Wheeler and Hendon (2004). According to the amplitude and phase information from RMM1 and RMM2, MJO events are divided into eight active phases that indicate the location of convective activity. To focus on the austral spring, we use the events that occurred between September and November to construct the MJO composites. "Active MJO days" are identified as days when the MJO's amplitude exceeds 1.5 (as in Yoo et al., 2012) for more than five consecutive days. The results are similar when the threshold varies within the range of 1.0–2.0. An "independent MJO event" is identified when consecutive active MJO days last for at least 5 days and are separated by at least 7 days from any other active MJO days within the same phase. Using these criteria, we identified 16 independent MJO Phase 8 (P8) events during September–November from 1979 to 2018 (see Table S1 in supporting information).

We will use the SD-WACCM4 output to evaluate the continuity equation of zonal-mean ozone concentration (e.g., Andrews et al., 1987). The continuity equation in the transformed Eulerian mean framework can be written as

$$\partial_t \overline{O_3} = -a^{-1}\bar{v}^*\partial_\phi \overline{O_3} - \bar{w}^*\partial_z \overline{O_3} + e^{z/H}(\nabla \cdot \boldsymbol{M}) + \overline{S}, \quad (1)$$

wwhere O_3 denotes the ozone mixing ratio. H is the scale height, a is Earth's radius, ϕ is latitude, and z is altitude. v^* and w^* in Equation 1 denote the TEM residual meridional and vertical winds defined as $v^* = \bar{v} - \rho_0{}^{-1}\left(\rho_0 \overline{v'\theta'}/\theta_z\right)_z$ and $w^* = \overline{w} + (a\cos\phi)^{-1}\left(\cos\phi\rho_0 \overline{v'\theta'}/\theta_z\right)_\phi$, respectively. The overbars indicate

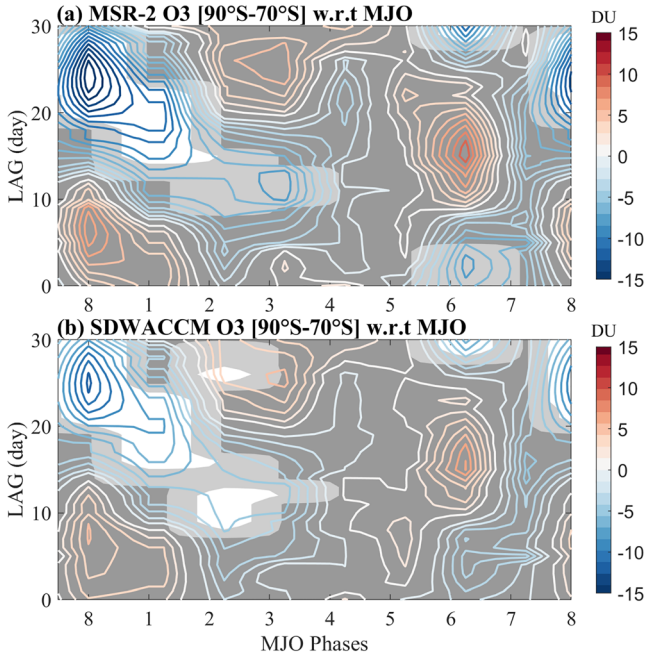

Figure 1. Antarctic total column ozone anomalies (DU) from MSR-2 at different lags with respect to MJO phases during September to November from 1979 to 2014. The white and light-gray areas denote significance at the 95% and 90% levels, respectively, according to the Student's *t* test. (b) is the same as (a) but for SD-WACCM simulation from 1979 to 2014. The contour intervals are 1 DU.

zonal means, primes are deviations from it, and subscripts denote partial derivatives. The total ozone tendency is divided into the change due to transport processes that occur due to advection by the residual circulation, the eddy effects ($\nabla \cdot \boldsymbol{M}$), and the net ozone tendency due to chemistry (chemical production minus loss, S). The vector $\boldsymbol{M}$ is the eddy flux term, which is defined as

$$\boldsymbol{M} = \begin{pmatrix} \boldsymbol{M}^y \\ \boldsymbol{M}^z \end{pmatrix} = \begin{pmatrix} -e^{Z/H}\left(\overline{v'O_3'} - \overline{v'\theta'}\,\partial_z\overline{O_3}/\partial_z\overline{\theta}\right) \\ -e^{Z/H}\left(\overline{w'O_3'} + a^{-1}\overline{v'\theta'}\,\partial_\phi\overline{O_3}/\partial_z\overline{\theta}\right) \end{pmatrix}. \quad (2)$$

Its divergence represents the diffusive effects of the eddies as well as additional advective effects that are not represented by the residual meridional circulation. The sum of the first three terms on the right-hand side of Equation 1 is the total ozone tendency from dynamics, while the last term of Equation 1 is the total ozone tendency due to chemistry.

To focus on the intraseasonal time scale, we remove both the long-term trend and the seasonal cycle of ozone, temperature, and dynamical parameters. Equivalent effective stratospheric chlorine is used to evaluate the long-term trend of ozone. The equivalent effective stratospheric chlorine time series used in this study corresponds to the WMO A1-2010 scenario and uses the method suggested by Newman et al. (2007). The long-term trends for temperature and dynamical variables are calculated with linear fits. The climatological mean seasonal cycle is based on the average for 1979–2014. After removing the long-term trend and seasonal variability, the intraseasonal variations in ozone and all dynamical variables are determined by applying 10–100 days band-pass filtering. Finally, these anomalies are used to form composites of the ozone and atmospheric variations during and after MJO phases.

3. Results

Figure 1 shows the anomalous TCO in the SH polar region (area weighted over 70°S and poleward) during each MJO phase as a function of time during the austral spring (SON) derived from the MSR-2 ozone reanalysis data set and SD-WACCM simulations. In the composite of MSR-2 reanalysis (Figure 1a), the SH TCO shows significant decreases with minima of approximately −15 DU seen 20–30 days after MJO P8 (16 cases) and 15–25 days after MJO P1. Enhanced ozone is evident ~20 days after Phase 6, though this effect is not statistically significant. The difference between negative and positive TCO anomalies reaches 22 DU, although the positive anomalies are not significant. There are also negative TCO anomalies 10 days after P2 and P3 (20 cases), and shortly after P6 (24 cases), which are all significant at the 90% level.

The SH polar TCO responses to the MJO in the SD-WACCM simulation (Figure 1b) are in good agreement with those in MSR-2 reanalysis. For the SD-WACCM simulation, the TCO anomalies are also significantly negative and lag MJO P8 by ~25 days; however, the magnitudes of the minima of −8 DU are smaller than those in MSR-2. The TCO anomalies in MJO P8&P1 are opposite to those in MJO P6. Also, note that the anomaly that lags MJO P6 in MSR-2 is significant only at the 90% level. The time evolution of the TCO response is consistent with the periodicity of the MJO. This suggests a statistically significant connection between the Antarctic TCO variations and certain MJO phases. The most significant Antarctic TCO response to MJO is seen 20–30 days after MJO P8 and 15–25 days after MJO P1. In the remainder of this study, both dynamical and chemical factors lagging MJO P8 are examined to probe the possible mechanism involved in the MJO link to Antarctic ozone.

It is worth noting that there are also significant TCO anomalies after MJO P1 at lags of ~20 days. Due to the cyclic nature of the MJO and the lag in the response, these MJO P1 and P8 cases often occur within the same MJO cycles. To account for this, the inactive MJO P8 events that are followed by an active P1 event are also identified as an active event. The category of active MJO P8 that includes inactive periods that are followed

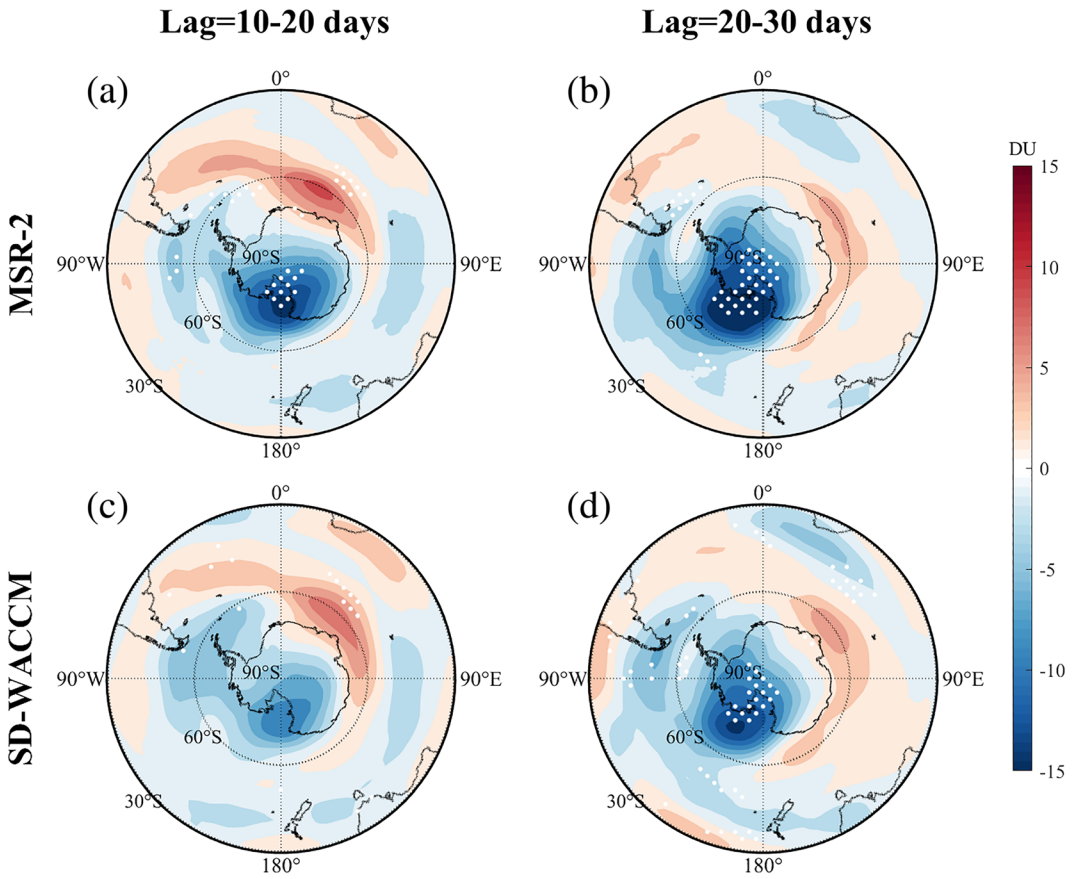

Figure 2. Southern hemispheric MSR-2 total column ozone (TCO) anomalies for (a) 10–20 days and (b) 20–30 days after the extended MJO P8. The contour intervals are 2 DU. Stippling indicates statistical significance at the 95% level according to the Student's *t* test. (c) and (d) are the same as (a) and (b) but for the SD-WACCM simulation.

by active P1 events is labeled as "extended MJO P8." Using this adjusted criterion for active MJO events, most of the active MJO P1 cases are also considered in the composite of MJO P8. There are 26 extended MJO P8 active cases (10 were added by the P1 extension just described) during SON from 1979 to 2014; only 4 among 23 active MJO P1 cases are excluded from the extended composite.

Figures 2a and 2b show the composition of MSR-2 TCO anomalies for 10–20 and 20–30 days after the extended MJO P8. In the SH polar region 10–20 days after the extended MJO P8, there is a region of significantly negative TCO anomalies centered at 70°S, 180° with the minimum of approximately −14 DU. The TCO anomalies in the eastern hemisphere (centered at 60°S, 30°E) are significantly positive and make up part of a wave-one pattern at 60°S. Twenty to 30 days after the extended MJO P8, the negative anomalies in TCO extend poleward and become more pronounced (−17 DU). Meanwhile, the wave-one pattern at approximately 60°S has shifted eastward; the negative anomalies are centered at 140°W and the positive anomalies at 60°E (although the positive anomalies are less significant at this lag). In the SD-WACCM simulation (Figure 2c), the pattern of SH TCO anomalies 10–20 days after the extended MJO P8 is similar to that in the MSR-2 reanalysis. However, the magnitude of the anomalies is generally smaller, and the negative anomalies in the polar region are not significant. From Days 20 to 30 after the extended MJO P8 (Figure 2d), the anomalous TCO in SD-WACCM suggests a significant decrease in the SH polar region, which agrees well with that in MSR-2. Since the TCO response to the MJO in the SD-WACCM simulations is in good agreement with that in the MSR-2 multi-satellite reanalysis, the dynamical and chemical processes in SD-WACCM are investigated to explore the possible mechanism by which the MJO modulates the SH TCO during certain phases.

The MJO has been shown to modulate PWs at middle and high latitudes in the troposphere (e.g., Matthews & Meredith., 2004); these in turn affect the stratosphere (e.g., Yang et al., 2017). The anomalies in polar

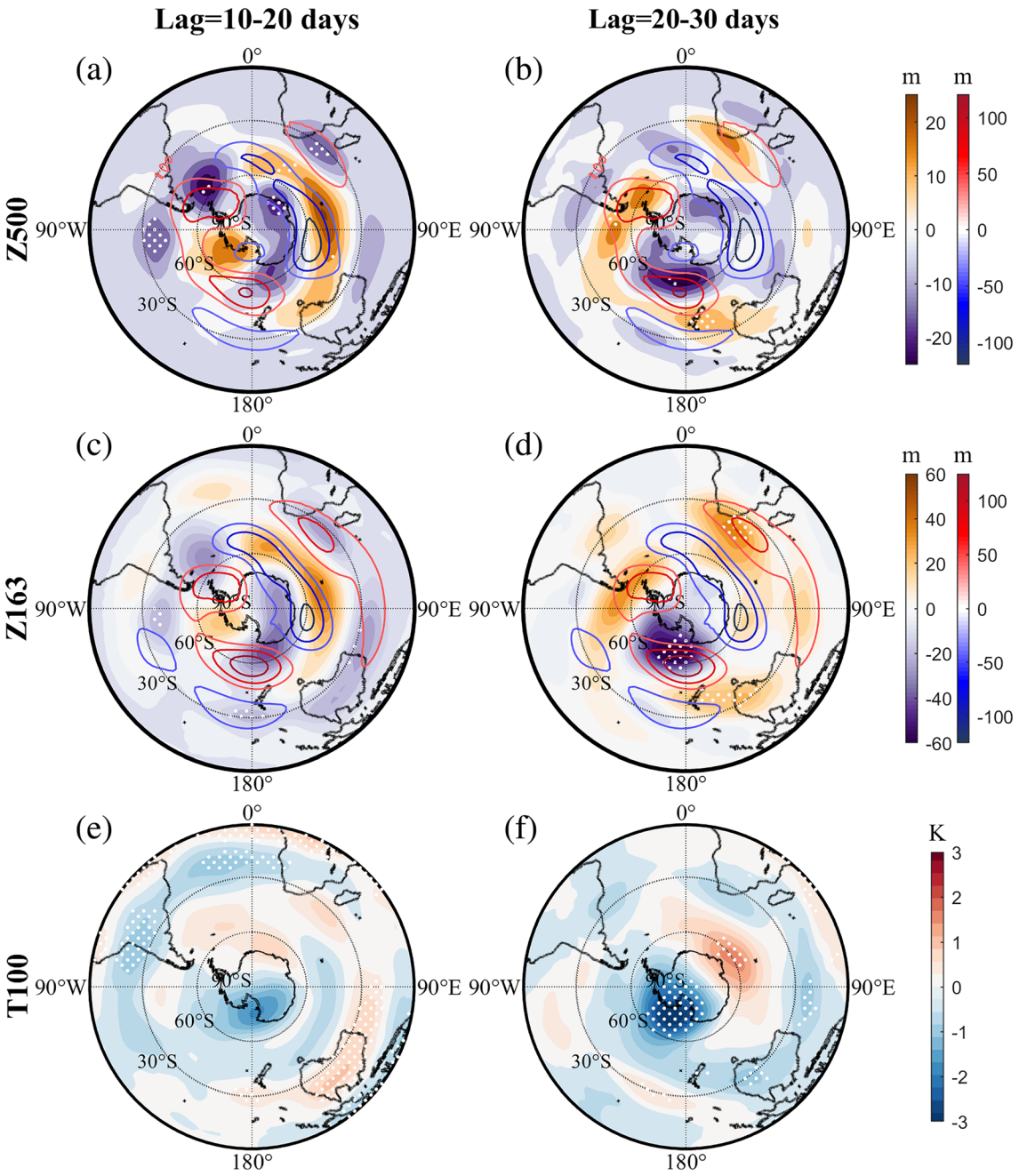

Figure 3. September–November climatological mean of 500-hPa geopotential height departure from zonal mean (contours) and geopotential height anomalies (shading) during (a) 10–20 days and (b) 20–30 days after the extended MJO P8 (shading) from SD-WACCM simulation. Stippling indicates statistical significance at the 95% level according to the Student's *t* test. (c) and (d) are the same as (a) and (b) but for 163-hPa geopotential height; 100-hPa temperature residuals during (e) 10–20 days and (f) 20–30 days after the extended MJO P8.

stereographic charts of 500-hPa geopotential height (Z), 169-hPa Z, and 100-hPa temperature (T) are investigated to explore the dynamical nature of the TCO response to MJO. As extratropical TCO is more readily relatable to temperature anomalies than to height anomalies, the anomalies in temperature are used to investigate the variations in the SH polar vortex. Here 100-hPa Z is not shown since it is similar to the 100-hPa T patterns.

Ten to 20 days after MJO P8 (Figure 3a), an anomalous cyclone at 500 hPa near 30°S over South Africa stretches southeastward across the Southern Indian Ocean toward Australia. Poleward of the low at South

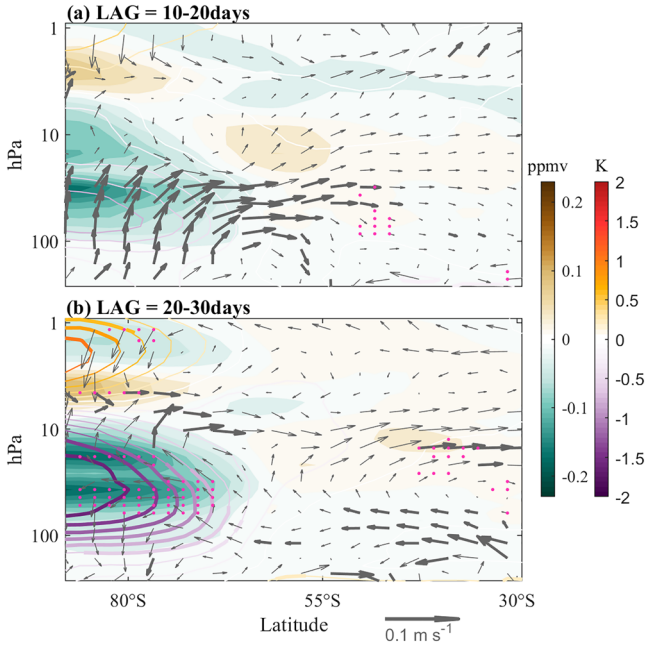

Figure 4. Composite of the zonal-mean ozone mixing ratio (ppmv, shading), the zonal-mean temperature (K, contours), and residual circulation (gray vectors) anomalies in SD-WACCM during (a) 10–20 days and (b) 20–30 days after the extended MJO P8. The violet dots indicate that the ozone anomalies are significant at the 95% level according to the Student's *t* test. The thick contours and the thick vectors indicate that the temperature and the residual circulation anomalies are significant at the 95% level.

Africa and the South Indian Ocean is a ridge at 40–50°S and a trough at 70°S, which suggests an anomalous wave train that emanates from the subtropical South Indian Ocean to the SH polar region. These extratropical Rossby wave trains are consistent with the wave trains induced by anomalous MJO convection (e.g., Matthews & Meredith., 2004; Yang et al., 2017) and are similar to the PW induced by El Niño-like sea surface temperature anomalies (Lin et al., 2012). The anomalous wave train from Days 10 to 20 after the extended MJO P8 (Figure 3a) is nearly out of phase with the climatological mean distribution in the SH extratropical troposphere, indicating suppressed PW activity. The geopotential height anomalies in the SH extend well into the lower stratosphere (Figure 3c) and coincide with the striking warm *T* anomalies at 100 hPa over Australia (Figure 3e) and cold anomalies south of Australia at around 50°S. The SH polar region exhibits a wave-one pattern with positive *T* anomalies over high latitudes of the South Atlantic and Indian Ocean sectors and negative anomalies over the Pacific sector, although it is not significant. The barotropic warm and cold anomalies coincide closely with the ozone maximum and minimum in Figure 2.

In the subtropics, the pattern of anomalous *Z* 20 to 30 days after the extended MJO P8 (Figures 3b and 3d) has rotated eastward relative to that during Days 10 to 20. Significant positive anomalies are seen east of Australia near 160°E, 30°S and negative anomalies are centered at 160°W, 60°S. In the SH polar region, anomalies in both *Z* and *T* (Figures 3b, 3d, and 3f) are amplified and become significant. The wave-one pattern in the SH high latitudes also rotates ~30° to the east; the pattern now shows positive *T* anomalies over high latitudes of the Indian Ocean and negative anomalies around 90°W–180°.

As a result of the suppressed PWs (Figures 3a and 3b), the residual mean meridional circulation in the SH lower stratosphere (Figure 4a) is characterized by equatorward anomalies between 50°S and 70°S 10–20 days after the extended MJO P8. This implies that the increase in ozone due to transport from midlatitudes to the polar region is weakened in the lower SH stratosphere. In turn, the zonal-mean anomalous ozone mixing ratio becomes significantly negative 20–30 days after the extended MJO P8 at the SH polar cap region, with the minimum located at 50–100 hPa, 70–90°S (Figure 4b). In the SH polar region, during Days 10–20 after the extended MJO P8, there is significant anomalous upwelling below 10 hPa and anomalous downwelling above, although the downwelling in the upper stratosphere is not significant. The meridional residual circulation anomalies become marginally significant between 50°S and 70°S in the lower stratosphere during Days 20-30 after the extended MJO P8. The stratospheric polar temperature anomalies become negative 10 to 20 days after the MJO P8 and reach a minimum of approximately −1.5 K at 30–50 hPa afterward (20 to 30 days) as a result of adiabatic cooling induced by anomalous upwelling of the residual circulation. The stratospheric temperature response is similar to that induced by the warming pool El Niño (Hurwitz et al., 2011, 2013).

Figure 5 shows the corresponding transient evolution of the zonal-mean ozone tendencies averaged between 70°S and 90°S after the extended MJO P8. As noted earlier, the extratropical PW train excited by MJO in the troposphere could modulate the poleward transport of air mass in the lower SH stratosphere. As presented in Figure 5a, there is a pronounced negative ozone tendency in the high-latitude stratosphere 10 to 20 days after MJO P8 and a positive tendency beginning around 25 days. This negative stratospheric ozone tendency reaches its minimum value at 50 hPa on Day 15. The evolution of the total ozone tendency is consistent with the evolution of ozone transport, as indicated by the residual circulation (Figure 4b).

The colder Antarctic lower stratosphere that results from the PW anomalies is also expected to perturb the polar ozone by modulating the chemical ozone reactions, as suggested by previous studies (Brasseur &

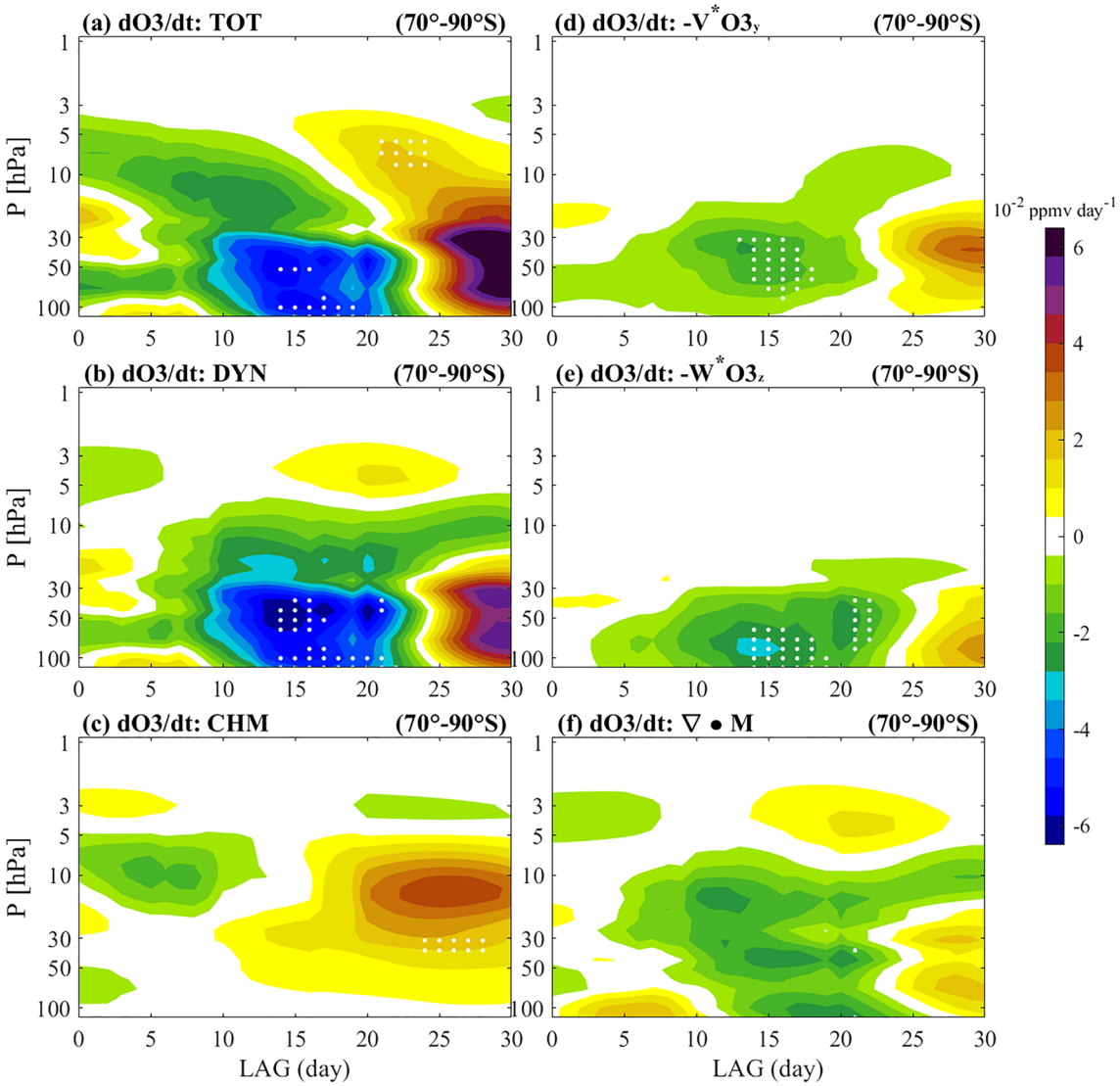

Figure 5. Evolution of the ozone tendencies (mass weighted with respect to 10 hPa) for the composite of 0–30 days after MJO Phase 8 as a function of time and pressure, averaged from 70°S to 90°S from SD-WACCM: (a) total ozone tendency and (b) ozone tendency anomaly due to dynamics and (c) due to parameterized chemistry. Tendency due to dynamics is decomposed into (d) vertical advection, (e) meridional advection, and (f) eddy transport effects. Stippling indicates statistical significance at the 95% level according to the Student's *t* test.

Solomon, 2005; Solomon et al., 2015). Thus, we analyze the implication of transient changes in residual circulation induced by MJO P8 on polar stratospheric ozone chemistry.

To investigate the source of the transient changes in polar stratospheric ozone after the extended MJO P8, we decompose the total ozone tendency into contributions from dynamics and chemistry. We find that anomalies in the evolution of the total ozone tendency in the middle-lower Antarctic stratosphere (between 10 and 100 hPa) are dominated by the dynamical terms (Figure 5b). The ozone tendency due to dynamics in the middle-lower stratosphere (100 and 10 hPa) is mainly due to the ozone transport via meridional (Figure 5d) and vertical (Figure 5e) advection by the residual circulation, while eddy transport also plays a role although the anomalies are only marginally significant (Figure 5f). The dominant role played by the dynamical terms in driving the anomalies in total ozone tendency is consistent with the transient changes in the residual mean transport. Conversely, the contribution of the chemistry to the anomalies in total ozone tendency (Figure 5c) is only significant at around 30 hPa at lags of approximately 25 days. The anomalous positive ozone tendency due to chemistry is likely associated with less chemical ozone loss due to decreased temperature there (Figure 4b). This is consistent with the ozone sink reactions in the middle-upper

stratosphere, which are strongly dependent on temperature (Brasseur & Solomon, 2005). However, the magnitude is relatively weak compared to that caused by dynamics. These results suggest that MJO-induced transient changes in the polar stratospheric ozone are primarily due to changes in dynamical ozone transport.

4. Conclusions

A significant connection is revealed between the Antarctic TCO and certain MJO phases (P1 and P8), as suggested by multi-satellite assimilation and a whole atmosphere model simulation. The difference between the negative and positive TCO anomalies in the SH polar region reaches 20 DU over the period 0 to 30 days after MJO P8. There is also a wave-one response of TCO in the middle latitudes of the SH. During 10 to 20 days after MJO P8, the anomalous Z are nearly out of phase with the climatological mean distribution in the SH extratropical troposphere. An anomalous extratropical wave train propagates from the subtropical Indian Ocean to the high latitudes in the SH and leads to wave-one Z and T responses in the high latitudes. This thermal structure extends into the stratosphere in the SH polar region. The suppressed upward propagation of PWs leads to an equatorward anomalous residual circulation in the SH stratosphere, which results in a deceleration in the poleward air mass transport in the lower SH stratosphere. As a result, a significant negative ozone tendency is observed at 50 hPa, 70–90°S, which contributes to the negative anomaly in TCO 20–30 days after MJO P8.

The perturbations to the normal seasonal total ozone balance in the middle-lower Antarctic stratosphere (10–100 hPa) are dominated by the dynamical terms; the largest contributions are from the ozone transport via meridional and vertical advection by the residual circulation. The magnitude of transient changes due to chemistry is relatively weak compared with that caused by dynamics.

Data Availability Statement

The ERA-Interim reanalysis data were downloaded online (http://apps.ecmwf.int/datasets). The real-time multivariate MJO (RMM) index is available online (at http://www.bom.gov.au/climate/mjo/graphics/rmm.74toRealtime.txt). EOS MLS L2 version 4.2 is available online (at https://mls.jpl.nasa.gov/data/). The model outputs used in this work are archived on the Open Science Framework at https://doi.org/10.17605/OSF.IO/MW9H8 and are publicly available.

Acknowledgments

This work is supported by the Strategic Priority Research Program of Chinese Academy of Sciences, Grant XDB 41000000, the National Natural Science Foundation of China (NSFC) (Grants 41874180, 41674149, 41974175, 41831071, and 41874181), and the Open Research Project of Large Research Infrastructures of CAS—"Study on the interaction between low/mid-latitude atmosphere and ionosphere based on the Chinese Meridian Project." We thank ECMWF for daily reanalysis data. The National Center for Atmospheric Research (NCAR) is sponsored by the National Science Foundation. WACCM is a component of the Community Earth System Model (CESM), which is supported by the National Science Foundation (NSF) and the Office of Science of the U.S. Department of Energy. Computing resources were provided by NCAR's Computational and Information Systems Laboratory (CISL).

References

Andrews, D. G., Holton, J. R., & Leovy, C. B. (1987). Middle atmosphere dynamics. In *Vol. 40 of International Geophysics Series* (p. 489). Cambridge, MA: Academic Press.

Brasseur, G., & Solomon, S. (2005). *Aeronomy of the middle atmosphere: Chemistry and physics of the stratosphere and mesosphere* (Vol. 5, 1st ed.). Dordrecht, Holland: Atmospheric and Oceanographic Sciences Library, Springer Netherlands.

Calvo, N., Polvani, L. M., & Solomon, S. (2015). On the surface impact of Arctic stratospheric ozone extremes. *Environmental Research Letters*, *10*(9), 094003. https://doi.org/10.1088/1748-9326/10/9/094003

Feldstein, S. B. (2011). Subtropical rainfall and the Antarctic ozone hole. *Science*, *332*(6032), 925–926. https://doi.org/10.1126/science.1206834

Ferranti, L., Palmer, T. N., Molteni, F., & Klinker, E. (1990). Tropical-extratropical interaction associated with the 30–60 day oscillation and its impact on medium and extended range prediction. *Journal of the Atmospheric Sciences*, *47*(18), 2177–2199. https://doi.org/10.1175/1520-0469(1990)047<2177:TEIAWT>2.0.CO;2

Fusco, A. C., & Salby, M. L. (1999). Interannual variations of total ozone and their relationship to variations of planetary wave activity. *Journal of Climate*, *12*, 1619–1629. http://doi.org/10.1175/1520-0442(1999)012<1619:IVOTOA>2.0.CO;2

Garcia, R. R., Marsh, D. R., Kinnison, D. E., Boville, B. A., & Sassi, F. (2007). Simulation of secular trends in the middle atmosphere, 1950–2003. *Journal of Geophysical Research*, *112*, D09301. https://doi.org/10.1029/2006JD007485

Garcia, R. R., Smith, A. K., Kinnison, D. E., de la Camara, A., & Murphy, D. (2017). Modification of the gravity wave parameterization in the Whole Atmosphere Community Climate Model: Motivation and results. *Journal of Atmospheric Science*, *74*(1), 275–291. http://doi.org/10.1175/JAS-D-16-0104.1

Garfinkel, C. I., Benedict, J. J., & Maloney, E. D. (2014). Impact of the MJO on the boreal winter extratropical circulation. *Geophysical Research Letters*, *41*, 6055–6062. http://doi.org/10.1002/2014GL061094

Gillett, Z. E., Arblaster, J. M., Dittus, A. J., Deushi, M., Jöckel, P., Kinnison, D. E., et al. (2019). Evaluating the relationship between interannual variations in the Antarctic ozone hole and Southern Hemisphere surface climate in chemistry–climate models. *Journal of Climate*, *32*(11), 3131–3151. https://doi.org/10.1175/JCLI-D-18-0273.1

Hurrell, J. W., Holland, M. M., Gent, P. R., Ghan, S., Kay, J. E., Kushner, P. J., et al. (2013). The Community Earth System Model: A Framework for Collaborative Research. *Bulletin of the American Meteorological Society*, *94*(9), 1339–1360. https://doi.org/10.1175/bams-d-12-00121.1

Hurwitz, M. M., Garfinkel, C. I., Newman, P. A., & Oman, L. D. (2013). Sensitivity of the atmospheric response to warm pool El Niño events to modeled SSTs and future climate forcings. *Journal of Geophysical Research: Atmospheres*, *118*, 13,371–13,382. https://doi.org/10.1002/2013JD021051

Hurwitz, M. M., Song, I. S., Oman, L. D., Newman, P. A., Molod, A. M., Frith, S. M., & Nielsen, J. E. (2011). Response of the Antarctic stratosphere to warm pool EI Nino events in the GEOS CCM. *Atmospheric Chemistry and Physics*, *11*(18), 9659–9669. https://doi.org/10.5194/acp-11-9659-2011

Kang, S. M., Polvani, L. M., Fyfe, J. C., & Sigmond, M. (2011). Impact of polar ozone depletion on subtropical precipitation. *Science*, *332*(6032), 951–954. https://doi.org/10.1126/science.1202131

Kang, W., & Tziperman, E. (2017). More frequent sudden stratospheric warming events due to enhanced MJO forcing expected in a warmer climate. *Journal of Climate*, *30*(21), 8727–8743. https://doi.org/10.1175/JCLI-D-17-0044

Kang, W., & Tziperman, E. (2018). The MJO-SSW teleconnection: Interaction between MJO-forced waves and the mid-latitude jet. *Geophysical Research Letters*, *45*(9), 4400–4409. https://doi.org/10.1029/2018GL077937

Kunz, A., Pan, L. L., Konopka, P., Kinnison, D. E., & Tilmes, S. (2011). Chemical and dynamical discontinuity at the extratropical tropopause based on START08 and WACCM analyses. *Journal of Geophysical Research*, *116*, D24302. https://doi.org/10.1029/2011JD016686

Lin, P., Fu, Q., & Hartmann, D. L. (2012). Impact of tropical SST on stratospheric planetary waves in the Southern Hemisphere. *Journal of Climate*, *25*(14), 5030–5046. https://doi.org/10.1175/JCLI-D-11-00378.1

Lin, J., & Qian, T. (2019). Impacts of the ENSO Lifecycle on Stratospheric Ozone and Temperature. *Geophysical Research Letters*, *46*, 10,646–10,658. https://doi.org/10.1029/2019gl083697

Longstreth, J. D., De, G., Kripke, M. L., Takizawa, Y., & van der Leun, J. C. (1995). Effects of increased solar ultraviolet radiation on human health. *Ambio*, *24*, 153–165.

Madden, R. A., & Julian, P. R. (1971). Detection of a 40–50 day oscillation in zonal wind in tropical Pacific. *Journal of the Atmospheric Sciences*, *28*, 702–708. https://doi.org/10.1175/1520-0469(1971)028<0702:DOADOI>2.0.CO;2

Madden, R. A., & Julian, P. R. (1972). Description of global-scale circulation cells in tropics with a 40–50 day period. *Journal of the Atmospheric Sciences*, *29*, 1109–1123. https://doi.org/10.1175/1520-0469(1972)029<1109:DOGSCC>2.0.CO;2

Marsh, D. R., Mills, M. J., Kinnison, D. E., Lamarque, J.-F., Calvo, N., & Polvani, L. M. (2013). Climate Change from 1850 to 2005 Simulated in CESM1(WACCM). *Journal of Climate*, *26*(19), 7372–7391. https://doi.org/10.1175/jcli-d-12-00558.1

Matthews, A. J., & Meredith, M. P. (2004). Variability of Antarctic circumpolar transport and the southern annular mode associated with the Madden-Julian oscillation. *Geophysical Research Letters*, *31*, L24312. https://doi.org/10.1029/2004GL021666

Newman, P. A., Kawa, S. R., & Nash, E. R. (2007). A new formulation of equivalent effective stratospheric chlorine (EESC). *Atmospheric Chemistry and Physics*, *7*(17), 4537–4552. https://doi.org/10.5194/acp-7-4537-2007

Randel, W. J. (1993). Global variations of zonal mean ozone during stratospheric warming events. *Journal of Atmospheric Science*, *50*, 3308–3321. https://doi.org/10.1175/1520-0469(1993)050<3308:GVOZMO>2.0.CO;2

Randel, W. J., Wu, F., & Stolarski, R. (2002). Changes in column ozone correlated with the stratospheric EP flux. *Journal of the Meteorological Society of Japan, Ser. II*, *80*, 849–862. https://doi.org/10.2151/jmsj.80.849

Rose, K., & Brasseur, G. (1985). Ozone During Sudden Stratospheric Warming: A Three-Dimensional Simulation. In C. S. Zerefos & A. Ghazi (Eds.), *Atmospheric Ozone* (pp. 28–32). Dordrecht: Springer Netherlands. https://doi.org/10.1007/978-94-009-5313-0_6

Salby, M., Titova, E., & Deschamps, L. (2011). Rebound of Antarctic ozone. *Geophysical Research Letters*, *38*, L09702. https://doi.org/10.1029/2011gl047266

Seo, K.-H., & Son, S.-W. (2012). The global atmospheric circulation response to tropical diabatic heating associated with the Madden-Julian Oscillation during northern winter. *Journal of the Atmospheric Sciences*, *69*(1), 79–96. https://doi.org/10.1175/2011JAS3686.1

Slaper, H., Velders, G. J., Daniel, J. S., de Gruijl, F. R., & van der Leun, J. C. (1996). Estimates of ozone depletion and skin cancer incidence to examine the Vienna Convention achievements. *Nature*, *384*, 256–258. https://doi.org/10.1038/384256a0

Smith, A. K., Garcia, R. R., Marsh, D. R., Kinnison, D. E., & Richter, J. H. (2010). Simulations of the response of mesospheric circulation and temperature to the Antarctic ozone hole. *Geophysical Research Letters*, *37*, L22803. https://doi.org/10.1029/2010GL045255

Solomon, S. (1999). Stratospheric ozone depletion: A review of concepts and history. *Reviews of Geophysics*, *37*, 275–316. https://doi.org/10.1029/1999RG900008

Solomon, S., Kinnison, D., Bandoro, J., & Garcia, R. (2015). Simulation of polar ozone depletion: An update. *Journal of Geophysical Research: Atmospheres*, *120*, 7958–7974. https://doi.org/10.1002/2015JD023365

Son, S. W., Polvani, L. M., Waugh, D. W., Akiyoshi, H., Garcia, R., Kinnison, D., et al. (2008). The impact of stratospheric ozone recovery on the Southern Hemisphere westerly jet. *Science*, *320*(5882), 1486–1489. https://doi.org/10.1126/science.1155939

Thompson, D., Solomon, S., Kushner, P. J., England, M. H., Grise, K. M., & Karoly, D. J. (2011). Signatures of the Antarctic ozone hole in Southern Hemisphere surface climate change. *Nature Geoscience*, *4*, 741–749. https://doi.org/10.1038/NGEO1296

Tian, W., Li, Y., Xie, F., Zhang, J., Chipperfield, M. P., Feng, W., et al. (2017). The relationship between lower-stratospheric ozone at southern high latitudes and sea surface temperature in the East Asian marginal seas in austral spring. *Atmospheric Chemistry and Physics*, *17*, 6705–6722. https://doi.org/10.5194/acp-17-6705-2017

van der A, R. J., Allaart, M. A. F., & Eskes, H. J. (2010). Multi sensor reanalysis of total ozone. *Atmospheric Chemistry and Physics*, *10*(22), 11,277–11,294. https://doi.org/10.5194/acp-10-11277-2010

van der A, R. J., Allaart, M. A. F., & Eskes, H. J. (2015). Extended and refined multi sensor reanalysis of total ozone for the period 1970–2012. *Atmospheric Measurement Techniques*, *8*(7), 3021–3035. https://doi.org/10.5194/amt-8-3021-2015

Van der Leun, J. C., Tang, X., & Tevini, M. (1995). Environmental effects of ozone depletion: 1994 assessment. AMBIO-STOCKHOLM-24, 138.

Wang, F., Tian, W., Xie, F., Zhang, J., & Han, Y. (2018). Effect of Madden-Julian oscillation occurrence frequency on the interannual variability of Northern Hemisphere stratospheric wave activity in winter. *Journal of Climate*, *31*(13), 5031–5049. https://doi.org/10.1175/JCLI-D-17-0476.1

Weber, M., Dikty, S., Burrows, J. P., Garny, H., Dameris, M., Kubin, A., et al. (2011). The Brewer-Dobson circulation and total ozone from seasonal to decadal time scales. *Atmospheric Chemistry and Physics*, *11*(21), 11,221–11,235. https://doi.org/10.5194/acp-11-11221-2011

Wheeler, M. C., & Hendon, H. H. (2004). An All-Season Real-Time Multivariate MJO Index: Development of an Index for Monitoring and Prediction. *Monthly Weather Review*, *132*(8), 1917–1932. https://doi.org/10.1175/1520-0493(2004)132<1917:aarmmi>2.0.co;2

Wirth, V. (1993). Quasi-stationary planetary waves in total ozone and their correlation with lower stratospheric temperature. *Journal of Geophysical Research*, *98*(D5), 8873–8882. https://doi.org/10.1029/92JD02820

Xie, F., Li, J., Tian, W., Fu, Q., Jin, F., Hu, Y., et al. (2016). A connection from Arctic stratospheric ozone to El Niño-Southern Oscillation. *Environmental Research Letters*, *11*, 124026. https://doi.org/10.1088/1748-9326/11/12/124026

Yang, C., Li, T., Smith, A. K., & Dou, X. (2017). Response of the Southern Hemisphere middle atmosphere to the Madden-Julian Oscillation during austral winter using the Specified-Dynamics Whole Atmosphere Community Climate Model. *Journal of Climate*, *30*(20), 8317–8333. https://doi.org/10.1175/JCLI-D-17-0063.1

Yoo, C., Lee, S., & Feldstein, S. B. (2012). Mechanisms of Arctic Surface Air Temperature Change in Response to the Madden–Julian Oscillation. *Journal of Climate*, *25*(17), 5777–5790. https://doi.org/10.1175/jcli-d-11-00566.1

Zhang, C. (2005). Madden-Julian oscillation. *Reviews of Geophysics*, *43*, RG2003. https://doi.org/10.1029/2004RG000158